Journal of Molecular Structure 1351 (2026) 144283

Contents lists available at ScienceDirect

Journal of Molecular Structure

journal homepage: www.elsevier.com/locate/molstr

Unveiling of the structural, optical and dielectric proprieties of cobaltite compound $La_{0.57}Nd_{0.1}Sr_{0.18}Ag_{0.15}CoO_3$for optoelectronic application

T. Benslimen [a], H. Issaoui [a,b], M. Brahmi [a], F. Issaoui [a,b,*], E. Dhahri [b], Benilde F.O. Costa [c], Bernardo A. Nogueira [d], Rui Fausto [d,e]

[a] Laboratory of Physics of Materials and NanomaterialsApplied to the Environment (LaPhyMNE),Faculty of Science and Technology of Sidi Bouzid, Kairouan University, 9100 Sidi Bouzid, Tunisia
[b] Laboratoire de Physique Appliquée, Faculté des Sciences de Sfax, B.P 1171, Tunisie
[c] University of Coimbra, CFisUC, Department of Physics, 3004-516 Coimbra, Portugal
[d] University of Coimbra, CQC, Department of Chemistry, 3004-535 Coimbra, Portugal
[e] Spectroscopy@IKU, Faculty of Sciences and Letters, Department of Physics, Istanbul Kultur University, Ataköy Campus, Bakirköy 34156, Istanbul, Türkiye

ARTICLE INFO

Keywords:
Sol-Gel
X-ray diffraction
Absorption
Band gap Eg impedance spectroscopy

ABSTRACT

In this research, we focus on the structural, morphological, magnetic and dielectric properties of **$La_{0.57}Nd_{0.1}Sr_{0.18}Ag_{0.15}CoO_3$(LNSACO)** compound synthesized by the sol-gel technique. The study by X-ray diffraction shows this compound crystallizes in the rhombohedral system, with R-3c space group. However, the XRD spectra reveal the existence of other peaks associated with the secondary phase of Co_3O_4 of space group Fd-3 m. The value of the optical band gap energy was determined from the variation of the absorbance as a function of the wavelength, this energy gap (Eg) of 1.46 eV. Electrical and dielectric characterizations of the material were performed using complex impedance spectroscopy in the frequency range from 100 Hz to 1 MHz and in a temperature range from 100 to 200 K. The conductivity spectra have been investigated by the Jonscher's law $\sigma(\omega)=\sigma_{dc}+A\omega^s$ with an increase in the frequency exponent (s) as the temperature increases. The imaginary part of the complex impedance (Z'') frequency dependence was characterized by the appearance of a peak, which moves towards higher frequencies with the increase in temperature. The activation energy values obtained from both dc conductivity and the impedance (Z″) spectrum are found to be very similar. Hence, the relaxation process may be attributed to the same type of charge carriers. The Z′ and Z″ versus frequency plots revealed the appearance of a semi-circular arcs and an electrical equivalent circuit of the type [(R1//CPE)(R2//C)] has been proposed to explain the impedance results.

1. Introduction

We substituted Co for manganese as the B-site cation in light of the positive magnetic results published by H. Issaoui [1]. Cobalt, a transition metal belonging to the iron group, has the electronic structure [Ar] 4s2 3d7. The physical characteristics of cobalt are very similar to those of nickel and iron. Compared to iron, it is less reactive chemically. Additionally, cobalt belongs to group 9, which is made up of the first three elements (Co, Rh, and Ir). Incomplete d-sublayers are what give most compounds their distinctive electrical and magnetic characteristics. Therefore, the root of particularly intriguing electron mobility events is the potential to stabilize various oxidation states within the same material [2].

The selection of 3D transition metals is the source of their remarkable qualities. Since the 1970s, a lot of research has been done on cobaltites with the general formula LnCoO3. The transition metal cobalt exhibits an assortment of oxidation states in this family of compounds, including Co2+/Co3+/Co4+, and may support a number of coordination geometries, including tetrahedral, octahedral, and square planar. Furthermore, cobalt exhibits a remarkable capacity to display a variety of spin states, in contrast to other 3D transition elements. The cation Co3+ (d4), for instance, can adopt Low Spin ($t_{2g}^6e_g^0$, $S=0$), Intermediate Spin ($t_{2g}^5e_g^1$, $S=1$), or High Spin ($t_{2g}^4e_g^2$, $S=2$) electronic configurations in an octahedral oxygen environment (O6) [3–5]. A characteristic of the cobaltites' perovskite structure that sets them apart from other three-dimensional metal oxides is their capacity to exist in three

* Corresponding author.
E-mail address: issawi_fatma@yahoo.fr (F. Issaoui).

https://doi.org/10.1016/j.molstruc.2025.144283
Received 9 June 2025; Received in revised form 8 September 2025; Accepted 5 October 2025
Available online 6 October 2025
0022-2860/© 2025 Elsevier B.V. All rights are reserved, including those for text and data mining, AI training, and similar technologies.

different spin states: low spin (BS), intermediate spin (SI), and high spin (HS). The formation of the mixed valence Co3+/Co4+ in the case of LnCoO3 is made possible by substituting a divalent cation, such as Ca2+, Ba2+, Sr2+, etc., for Ln3+. Therefore, the three configurations BS, SI, and HS can be arranged beneath each of these two cations, Co3+ and Co4+, which have $3d^6$ and $3d^5$ configurations, respectively.

The Co4+ cation is found in an intermediate spin configuration for SrCoO3 [6], admits the low spin state for BaCoO3 [7], and displays the low spin configuration for EuCoO3 [8].

Important optical parameters like the optical band gap and refractive index were found by using a material's optical behavior. Optical absorption spectra can be used to determine the material's indirect and direct band gap transitions.

Furthermore, electron transitions that occur when the valence band absorbs energy larger than the band gap (hv>Eg) are directly linked to optical characteristics. In the conduction band, this will be promoted [9].

Furthermore, the production procedures and fabrication technology have a significant impact on the optical physical properties of such substances. Optoelectronic applications, specifically light-emitting diodes (LEDs), may benefit from this. Certain materials allow for the selective and powerful absorption of UV radiation in the electromagnetic spectrum, opening up new research options to address this optical element.

In fact, because of their large gap energy (Eg = 3.24 eV and 3.3 eV, respectively), perovskites like PrCrO3 and SmCrO3 are among the compounds that can be used as basic materials for solid oxide fuel cells, UV photodetectors blind to solar radiation, UV photonic devices, and gas sensors [10–11]. Additionally, this synthesized samples have additional advantages such as excellent transparency, efficient light absorption, suitability for nonlinear applications, and most importantly, simple and cost-effective synthesis and to better understand the nature of electrical.

We added the element cobalt to the LNSACO molecule by conduction mechanisms. Impedance spectroscopy is used to investigate the dielectric characteristics of the resultant materials. In this section, we show that understanding how mobile charge carriers react after being excited by an electric current provides insight into transport mechanisms and makes a clear distinction between conductivity within grains and conductivity across grain boundaries.

In this work we focus on Cobalt-based oxides. It was prepared via sol gel method. properties of $La_{0.57}Nd_{0.1}Sr_{0.18}Ag_{0.15}CoO_3$were studied by RX, Raman. For this reason, we report the optical and dielectric properties of $La_{0.57}Nd_{0.1}Sr_{0.18}Ag_{0.15}CoO_3$.

2. Experimental procedureand characterization techniques

We used the sol-gel synthesis procedure to prepare the compound LNSACO.The precursors used are $La(NO_3)_3$, $Nd(NO_3)_3{\cdot}6H_2O$, $Sr(NO_3)_2$, $AgNO_3$, and $Co(NO_3)_2{\cdot}9H_2O$ of purity higher than 99.9 %. The equation of the synthesis reaction is the following:

$$0.57La(NO_3)_3 + 0.1Nd(NO_3)_3{\cdot}6H_2O + 0.18Sr(NO_3)_2 + 0.15AgNO_3 + Co(NO_3)_2{\cdot}6H_2O \Longrightarrow \mathbf{La_{0.57}Nd_{0.1}Sr_{0.18}Ag_{0.15}CoO_3 + 2.26O_2 + 12\,H_2 + 7.52NO_2}$$

The precursors are put in distilled water under magnetic stirring at 60 °C. To this mixture, citric acid and ethylene glycol are added with further heating at 170 °C until a brown gel is obtained. The oven-dried powder is firstly thoroughly ground for 30 min to obtain fine and homogeneous powder. The obtained powders are heated to temperatures of 600, 700 and 800 °C in air for 24 h with several grinding cycles in between.

The sample LNSACO was characterized by X-ray diffraction using a diffractometer equipped with a copper anti-cathode (Ȧ=1.5406 Å) [12]. The interpretation of the XRD spectra was carried out using the X-Pert High Score software. This software allows visualization of the XRD spectra of the samples with those of the standards. Moreover, with this software, the positions and the full widthat half maximum of the main peaks recorded were determined.

In order to have detailed information on the crystallographic structure of our sample, we resorted to the Rietveld refinement method [13]. Using the program "FullProf" developed by Rodrigez-Carjaval [14,15]. He microstructures and particle sizes were observed by a scanning electron microscope (S.E.M) which is a frequently used technique [16, 17].

A UV-3101PCscanning spectrophotometer with a dual-beam monochromator and two sources (a halogenlamp for the infrared range and a xenon lamp for the UV–visible range) was used to measure the optical properties at room temperature. This instrumentation has been used to measure the absorbance (*A*) in a wavelength range of 200–1200 nm.

3. Results and discussion

3.1. Structural characterization

3.1.1. X-ray diffraction patterns

X-ray diffraction was used to investigate the LNSACO sample using a diffractometer fitted with a copper anti-cathode (=1.5406 Å). At room temperature, an angular range of 10° to 100° with a step of 0.02° in 2° was used to record the X-ray pattern. Using the Full Prof program, the Rietveld method was used to refine the diffractogram that was produced for our drug.

Fig. 1 represents the experimental, calculated (refined) diffractograms, as well as the Bragg line positions of compound LNSACO. This diffractogram shows quite sharp and intense peaks which reflect a good crystallization of the sample of space group R-3c. On the other hand, this diffractogram shows the presence of a second minority phase Co_3O_4 of space group Fd-3 m which was identified with the help of X'PertHigh Score Plus software. This indicates that this temperature is not sufficient to obtain the chosen compound. The stars show the presence of the minority secondary phase which is linked to the impurity Co_3O_4. This impurity phase can significantly alter the magnetic and dielectric properties [18,19]. These impurities can disrupt the regular crystal structure, leading to changes in magnetic order and dielectric behavior. Specifically, the presence of impurities can influence the magnetic order of the material (e.g., from antiferromagnetic to weak ferromagnetic), affect the dielectric constant and losses, and charge carriers. but in our material the impurity phase of Co3O4 is very weak so it does not influence the dielectric properties.

The regular crystal structure may be upset by these impurities, changing the dielectric behavior and magnetic order. In particular, impurities can change the material's magnetic order (from antiferromagnetic to weak ferromagnetic, for example), charge carriers, and dielectric constant and losses. However, the Co3O4 impurity phase in our material is quite faint, therefore it has no effect on the dielectric characteristics.

The structure analysis was performed in the rhombohedral system with the space group $R\bar{3}C$ in positions 6a (0, 0, 1/4) for (La, Nd, Sr, Ag) atoms, 6b (0, 0, 0) for (Co) atoms, and 18e (1/2,0, 1/4) for oxygen.

The structural parameters obtained by refinement are reported in Table 1.

The refinement results are grouped in Table 1. In this table, we also noted the residual refinement values:*a ,b, c* the lattice parameters, $B_{iso}$the isotropic thermal agitation parameter, *x, y* et *z* the atomic positions, $d_{Co\text{-}O}$ the distance (cation-oxygen), $\boldsymbol{\Theta_{Co\text{-}O\text{-}Co}}$ the angle (oxygen-cation-oxygen), $\boldsymbol{\chi^2}$ the quality of the fit.

To validate the existence of the rhombohedral type structure and the degree of distortion of the structure of the LNSACO compound with respect to the ideal cubic structure. We have calculated the Goldschmidt tolerance factor [20] which is given by the following formula:

$$t = \frac{\langle r_A \rangle + r_O}{\sqrt{2}(\langle r_B \rangle + r_O)} \quad (1)$$

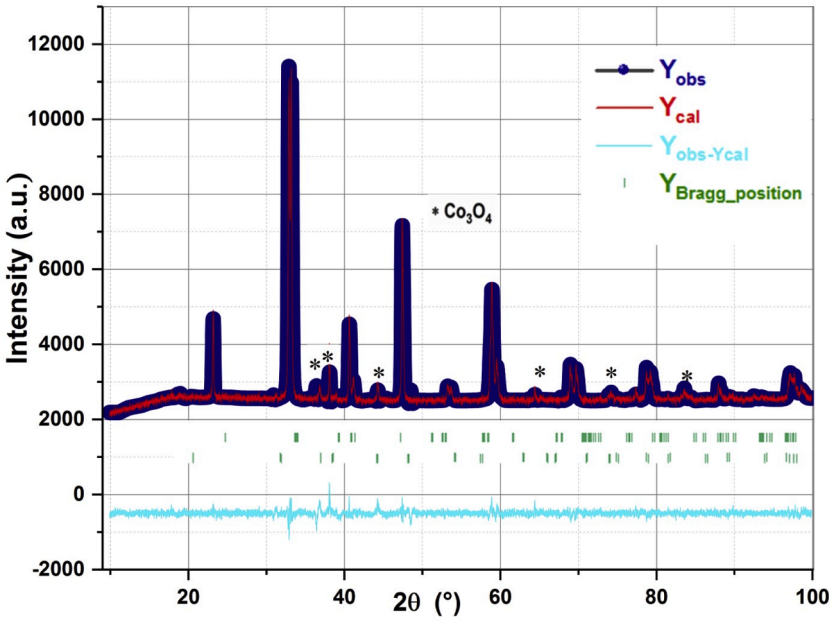

Fig. 1. The XRD Rietveld Refinement results of the compound $La_{0.57}Nd_{0.1}Sr_{0.18}Ag_{0.15}CoO_3$.

Table 1
Rietveld refinement results of the compound.

Compound				$La_{0.57}Nd_{0.1}Sr_{0.18}Ag_{0.15}CoO_3$	co_3
Group of space				***R 3- C***	***Fd-3m***
Parameters ofmesh	***a (Å)***			**5.442 (2)**	**8.183(2)**
	b (Å)			**5.442 (2)**	**8.183(2)**
	c (Å)			**13.156 (6)**	**8.183(2)**
	V (Å^3)			**337.44 (3)**	**548.08**
Atoms	***La/Sr/Nd/Ag***	**Wyckoff's positions**		**6[a]**	**4c**
		Atomicpositions	**x, y, z**	**(0.0.0.25)**	**(0.125.0.125.0.125)**
		Occupancyfactors		**0.1/0.57/0.18/0.15**	**1**
		B_{iso} (Å^2)		**0.57 (8)**	**1 (0)**
	Co	**Wyckoff's positions**		**6b**	**16d**
		Atomicpositions	**x, y, z**	**(0.0.0)**	**(0.5.0.5.0.5)**
		Occupancyfactors		**1**	**2**
		B_{iso} (Å^2)		**0.6 (1)**	**4.4(6)**
	O	**Wyckoff's positions**		**18e**	**32e**
		Atomic positions	**x, y, z**	**(0.5.0.0.25)**	**(0.43 (3) .0,25(3) .0.43(3))**
		Occupancyfactors		**3**	**4**
		B_{iso} (Å^2)		**1.9 (2)**	**2 (0)**
Settings Structural	***$D_{Co\text{-}O}$ (Å)***			**1.91574(6)**	
	$\Theta_{Co\text{-}O\text{-}Co}$ (°)			**180.0 (7)**	
Factors of agreement	***R_p (%)***			**1.90**	***R_p (%)***
	R_{wp} (%)			**2.53**	***R_{wp} (%)***
	R_F(%)			**3.28**	***R_F(%)***
	χ^2 (%)			**1.72**	***χ^2 (%)***
Atomic percentage of the phases				**99.88**	**0.15**

With: *rA*=*r*(*La,Nd,Sr,Ag*), *rB*= *r*(*Co*) and r_O are the ionic radii associated with the cations of sites A, B and oxygen, respectively.

For LNSACO, we have :

$$\langle r_A \rangle = 0.57\mathbf{r}_{La^{3+}} + 0.1\mathbf{r}_{Nd^{3+}} + 0.18\mathbf{r}_{Sr^{2+}} + 0.15\mathbf{r}_{Ag^{+}}$$

$$\langle \mathbf{r_B} \rangle = 0.52\mathbf{r}_{Co^{3+}} + 0.48\mathbf{r}_{Co^{4+}}$$

With: $\mathbf{r}_{La^{3+}}$ = 1.36 Å, $\mathbf{r}_{Nd^{3+}}$=1.27 Å, $\mathbf{r}_{Sr^{2+}}$ = 1.44 Å,$\mathbf{r}_{Ag^{+}}$ = 1.28 Å,$\mathbf{r}_{Co^{3+}}$ = 0.61 Å,$\mathbf{r}_{Co^{4+}}$ = 0.53 Å,$\mathbf{r}_O$ = 1.41 Å [20]

$$\langle \mathbf{r_A} \rangle = 1.3534\,\text{Å}$$

$$\langle \mathbf{r_B} \rangle = 0.5716\,\text{Å}$$

In this context, the value of t for our LNSACO sample is 0.98. This result is in agreement with the orthorhombic structure relative to the Rietveld refinement [21].

3.1.2. Morphological characterization

The morphology and grain size of the LNSACO compound were observed using a scanning electron microscope (Fig. 2). This image was subjected to a statistical grain size distribution study using Image-J software. Fig. 2 illustrates the outcome by plotting the number of grains (counts) vs particle size (nm). The compound LNSACO's grain size distribution is depicted in this picture as a Lorentzian profile (red solid line). Grain size ranges from 117 nm on average. The sample's micrograph shows a reasonably consistent morphology. EDX microanalysis was used to examine the sample's homogeneity and elemental makeup (Fig. 3). We observe that every chemical element added during elaboration is present, confirming that all precursors were incorporated

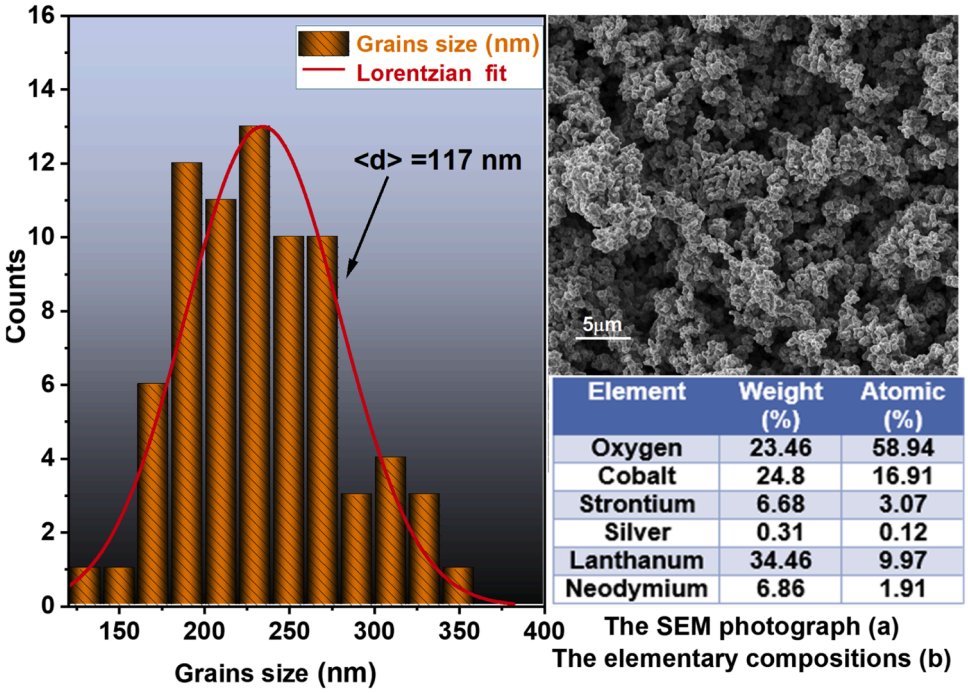

Element	Weight (%)	Atomic (%)
Oxygen	23.46	58.94
Cobalt	24.8	16.91
Strontium	6.68	3.07
Silver	0.31	0.12
Lanthanum	34.46	9.97
Neodymium	6.86	1.91

Fig. 2. Grain size distribution using << Image *J* >> software. Inset: SEM photo of compound $La_{0.57}Nd_{0.1}Sr_{0.18}Ag_{0.15}CoO_3$.

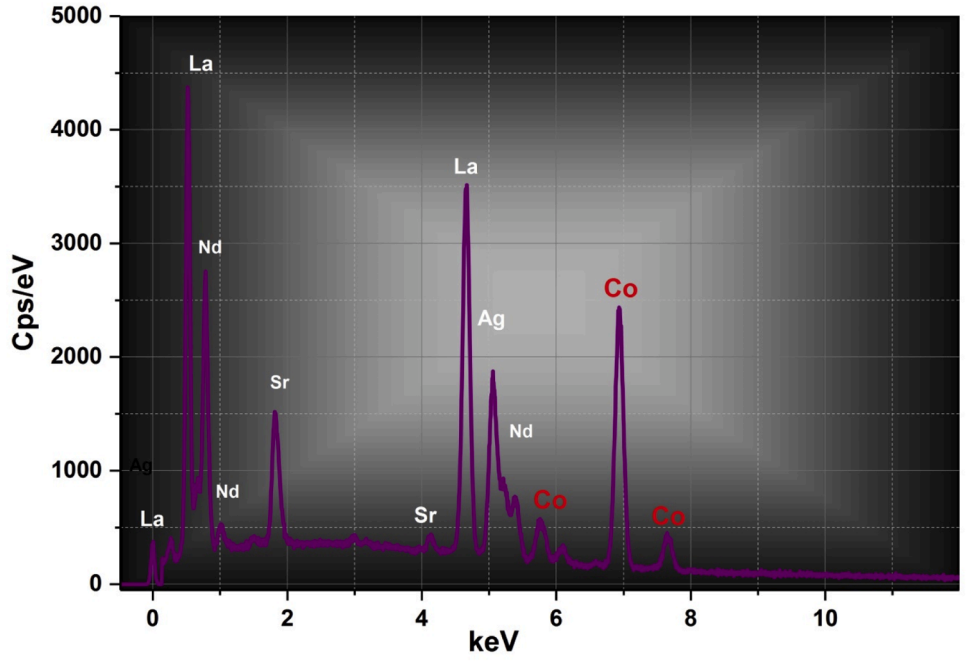

Fig. 3. Chemical analysis by EDX for $La_{0.57}Nd_{0.1}Sr_{0.18}Ag_{0.15}CoO_3$ compound.

throughout synthesis with no appreciable loss of volatile species at 800 °C. This analysis also verifies the stoichiometry of the compound and helps to check if we have soaked in the names of the samples during the preparation. Based on the results of EDX analysis of atomic percentages, we find the following formula $La_{0.62}Nd_{0.12}Sr_{0.19}Ag_{0.14}CoO_3$.

Similarly, we calculated the crystallite size using the Williamson-Hall approach [22] according to the following relationship:

$$\beta_{hkl}\cos\theta = \frac{k\lambda}{D_{wuL}} + 4\varepsilon\sin\theta \quad (2)$$

With: K the constant depends on the shape of the crystal ($K = 0.9$), λthe wavelength of the X-ray used, βthe width at the middle of the height of the highest intensity peak expressed in radians, Θdiffraction angle corresponding to the most intense peak and εis the average value of lattice strain [23–25].

For different diffraction peaks (hkl), β was measured. The typical crystallite size is D_(WH). Fig. 4 displays the curve for the Williamson-Hall (W-H) equation (βhkl cosθ= *f*(4 sinθ)). The linear fit's intercept is used to estimate the crystallite size D (WH) = 38,9477 nm, while the slope provides the induced strain (ε) Fig. 5.

The discrepancy between SEM and W-H results suggests that each grain observed by SEM is composed of several smaller crystallites.

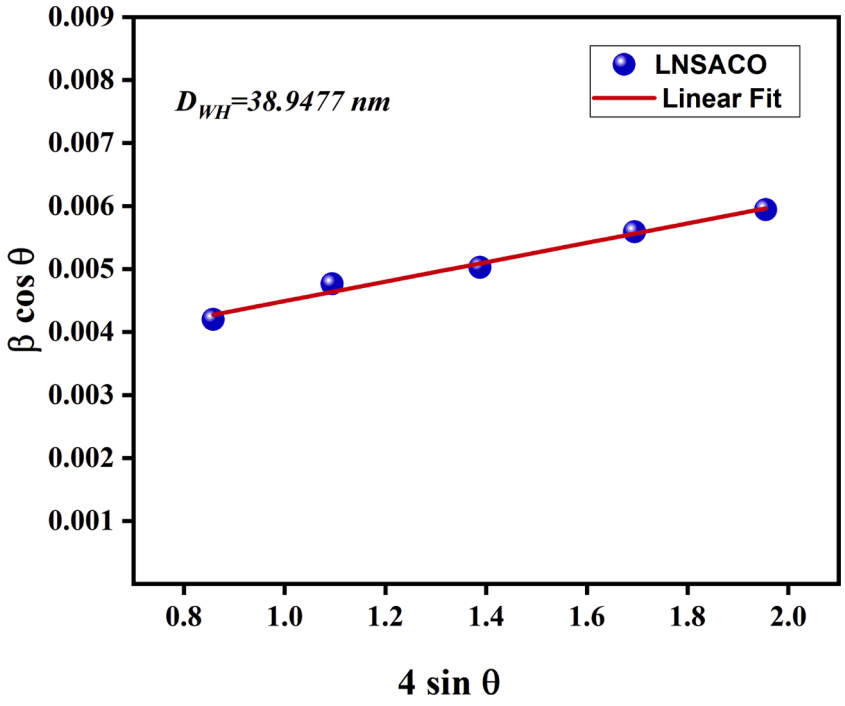

Fig. 4. Williamson-Hall analysis curve of $La_{0.57}Nd_{0.1}Sr_{0.18}Ag_{0.15}CoO_3$compound.

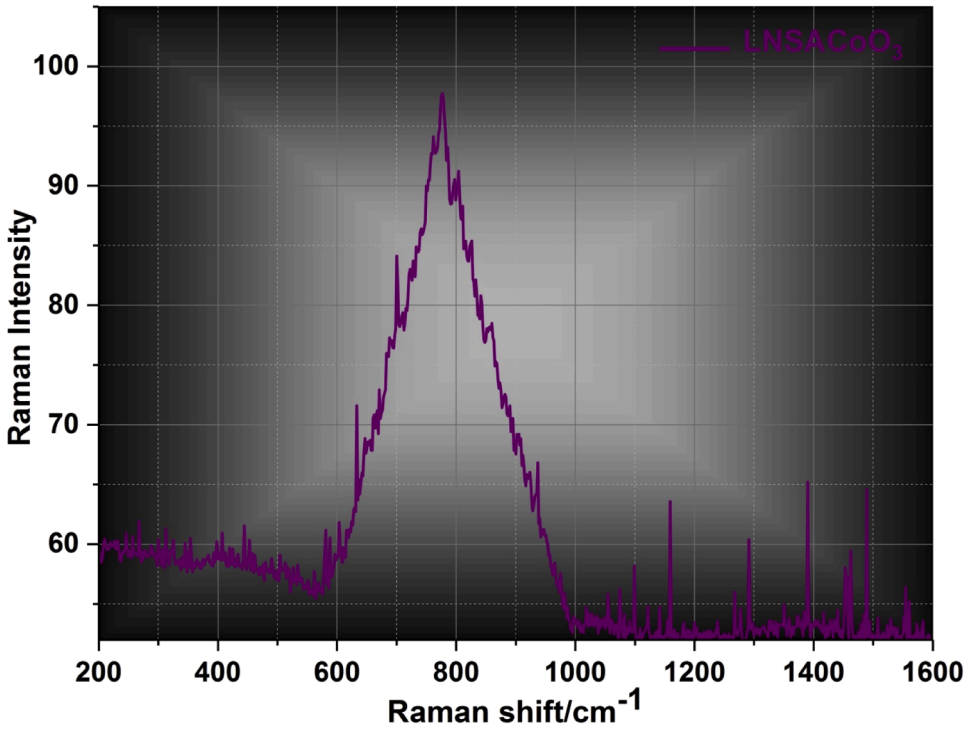

Fig. 5. Raman spectra for $La_{0.57}Nd_{0.1}Sr_{0.18}Ag_{0.15}CoO_3$compound.

3.1.3. Raman analysis

Raman spectra **were** obtained for the different samples using a Raman micro-system (Horiba LabRam HR Evolution), equipped with a Synapse CCD detector, a high-stability BXFM open space confocal microscope, and a 600 gr mm^{-1} grating, with 532 nm excitation. The laser power at the sample was approximately 17 mW, and the exposure time 30 s. A 50× objective lens was used. The final spectra are the mean of 60 scans for every sample. The wavelength used was 532 nm. displays the experimental Raman spectra of the investigated chemical in the wavenumber range 200 to 1600 cm $^{-1}$. The goal is to forecast vibrational frequencies and assign vibration modes to the perovskite group, which reveals 24 vibration modes [26]: ΓRaman = 7Ag + 5B1g + 7B2g + 5B3g (2). The active Raman modes are classified into five categories. Six Raman modes are associated with rotation/tilting of the octahedral BO6, four with bending, eight with motion in the ABO_3 of the A-site cations, two with symmetric stretching, and four with anti-symmetric stretching

[27]. Comparing the examined compound to the pure compound, however, reveals a slight variation in the total breadth at half maxima of a number of peaks.

3.2. Complex impedance spectroscopy

Fig. 6 represents the variation of the real part of the impedance (Z') as a function of the frequency at different temperatures for the LNSACO compound. We notice that the impedance values are relatively high for low frequencies. These values gradually decrease with increasing frequency, indicating enhanced electrical conductivity. This behavior is mainly due to the increase in the mobility of the charge carriers and the decrease in the density of trapped charges within the material [28]. At higher frequencies, the impedance curves tend to merge, indicating a possible release of space charge due to the lowering of the barrier properties of the material at higher temperatures and can be interpreted by the presence of space charge polarization [29]. The variation of the imaginary part of the impedance (Z'') as a function of frequency at different temperatures has been studied, and the results are shown in Fig. 7. The spectra of Z'' are characterized by the appearance of peaks Z''_{max} at frequencies f_{max} varying with the temperature. These peaks move towards high frequencies with increasing temperature, indicating the presence of a relaxation phenomenon in our material [30]. Moreover, one can also notice that the amplitude of Z'' decreases progressively while increasing the temperature. This may be due to an accumulation of space charges in both compounds [31,32].

In order to estimate the characteristic activation energy of the relaxation process, we represent in Fig. 8 the variation logarithmic relaxation frequencies as a function of 10^3/T. The temperature dependence of the relaxation frequency follows Arrhenius' law:

$$f_{max} = f_0 exp\left(\frac{E_a}{k_B T}\right) \quad (3)$$

In the above equation, f_0 is the pre-exponential factor, $E_a$is the activation energy and k_B is Boltzmann's constant.

The slope of the fitted lines allowed us to calculate the activation energies of our sample. The values found are equal to 0.105 eV.

3.3. Nyquist diagrams and equivalent electrical circuits

Fig. 9 shows the Nyquist diagrams at different temperatures of the compound LNSACO. The impedance spectra are described by circular arcs whose centers are located below the real axis. This suggests that the conduction in these materials can be described by the Cole-Cole model.

In addition, any increase in temperature is accompanied by a decrease in the diameter of the arcs of the circles, which leads to an improvement in conductivity [33]. We used the Z-View software to model these spectra by an equivalent electrical circuit in order to describe the electrical behavior of our materials [34]. As illustrated in Fig. 10, the best fit is achieved by employing an analogous electrical circuit made up of a series combination of two contributions: one for the grains (Rg-Cg) and one for the grain borders (Rjg-CPEjg) (where CPE is the constant phase element).The altered parameters' values. demonstrate that our samples exhibit semiconductor behavior when the values of the grain boundary resistance drop with increasing temperature, from 75.6 × 105Ω at 100 K to 0.15×105Ω at 200 K [35]. Furthermore, it has been discovered that Rjg values are greater than Rg values. For instance, at 150 K, $R_{jg} = 1.61\times105\Omega$, whereas $R_g = 6.24\times105\Omega$. This is explained by the chaotic atomic arrangement close to the grain boundaries, which increases electron scattering.

3.4. Study of electrical conductivity

In order to understand the behavior of electrical conduction and to determine the parameters that can control conduction processes in $La_{0.57}Nd_{0.1}Sr_{0.18}Ag_{0.15}CoO_3$(LNSACO), variations of conductivity as a function of frequency at different temperatures ranging from 100 K to 200 K is shown in Fig. 11. As seen in this figure, conductivity increases with increasing frequency and temperature. We also notice that at low frequencies, the spectra of the conductivity are independent of the frequency for each temperature. At high frequencies, the conductivity increases with increasing frequency. According to Jonscher's law [36], the frequency dependence of conductivity is expressed as:

$$\sigma_{ac}(\omega) = \frac{\sigma_S}{1+\tau^2\omega^2} + \frac{\sigma_\infty \tau^2\omega^2}{1+\tau^2\omega^2} + A\omega^S \quad (4)$$

In the above equation, σ_S is the conductivity at low frequencies, $\sigma_\infty$is

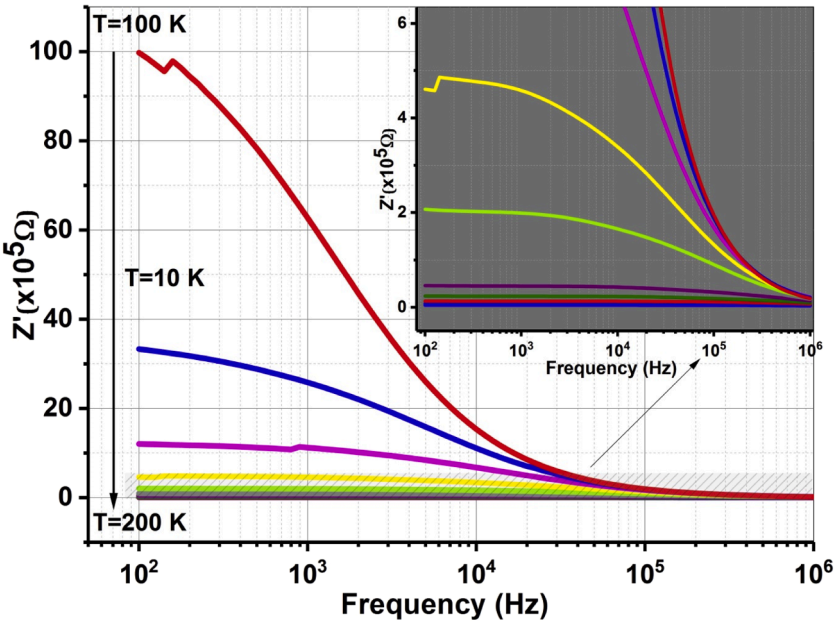

Fig. 6. The frequency dependence of the real part (Z') of the complex electrical impedance at several measurement temperatures for $La_{0.57}Nd_{0.1}Sr_{0.18}Ag_{0.15}CoO_3$compound.

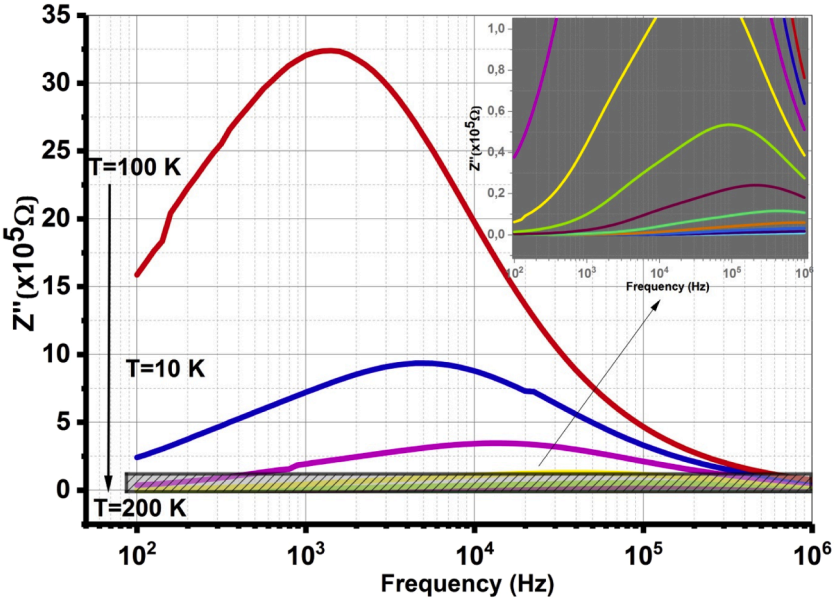

Fig. 7. The frequency dependence of the imaginary part (Z'') of the complex electrical impedance at several temperatures for $La_{0.57}Nd_{0.1}Sr_{0.18}Ag_{0.15}CoO_3$compound.

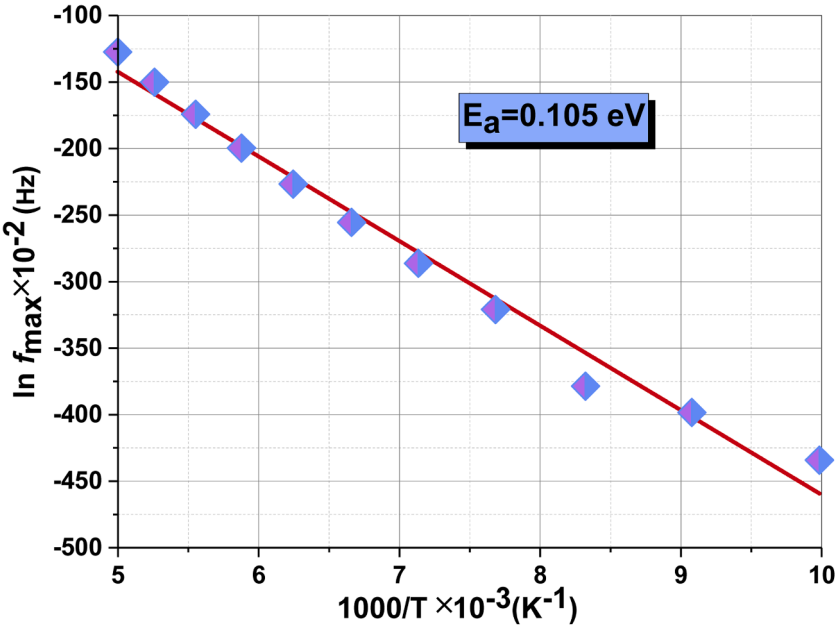

Fig. 8. Logarithmic variation of relaxation frequencies corresponding to as a function of 103/T of$La_{0.57}Nd_{0.1}Sr_{0.18}Ag_{0.15}CoO_3$compound.

an estimate of conductivity at high frequencies, ω is the angular frequency, τ represents the characteristic relaxation time, A is a constant temperature dependent, and $s$is the power law exponent, where $0 < s < 1$. Represents the degree of interaction between the mobile ions with the environments surrounding them, and A determines the strength of polarizability.

The behavior of the frequency exponent s as a function of temperature, obtained from fitting of experimental data with Eq. (4), can be used to determine the origin of conduction mechanism. Several models [37, 38] based on classical hopping of charge carriers over barrier and quantum mechanical tunneling have been proposed to investigate the conduction mechanism on the basis of variation of frequency exponent with temperature. So, temperature dependence of s plays a key role in the estimation of the conduction mechanism.

According to the quantum mechanical tunneling (QMT) model [39], the exponent 's' is practically equal to 0.8 and increases slightly with increasing temperature. It is given by the expression:

$$s = 1 + \frac{4}{\ln(\omega\tau 0)} \tag{5}$$

With τ_0 the relaxation time.

According to the wide overlap polaron tunneling (OLPT) model [40], the exponent 's' is both temperature and frequency dependent. It decreases with temperature from unity to a minimum value, and then increases.

According to the Correlation Barrier Hopping (CBH) model, the values of the frequency exponent 's' decrease with increasing temperature [41] according to the formula:

$$s = 1 - \frac{6kBT}{WM + k_B T \ln \omega\tau 0} \tag{6}$$

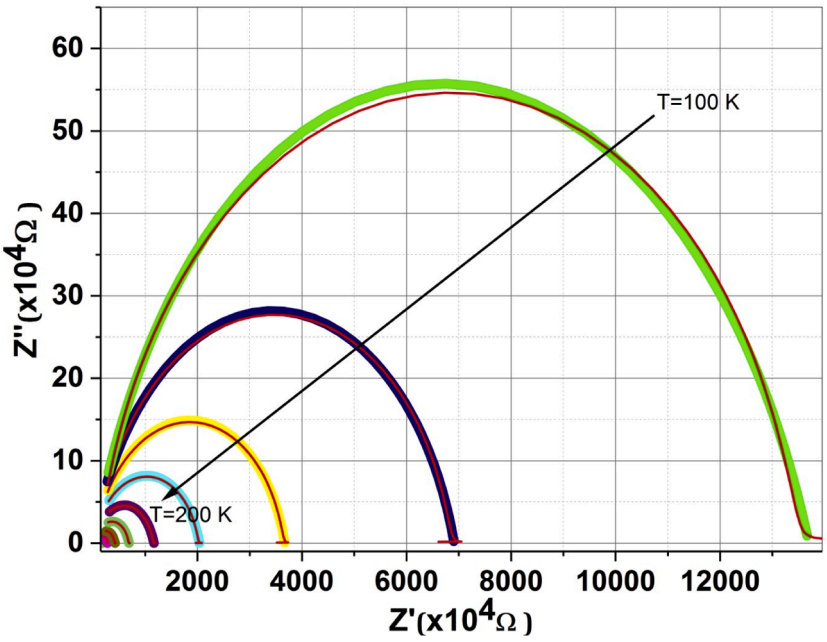

Fig. 9. Complex impedance spectrum at different temperatures for $La_{0.57}Nd_{0.1}Sr_{0.18}Ag_{0.15}CoO_3$compound.

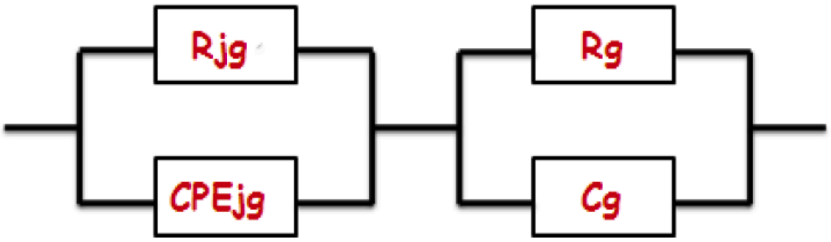

Fig. 10. The equivalent circuit formed by a parallel combination of grain resistance (R-C1 circuit) and constant phase element impedance (ZCPE) (R-CPE circuit).

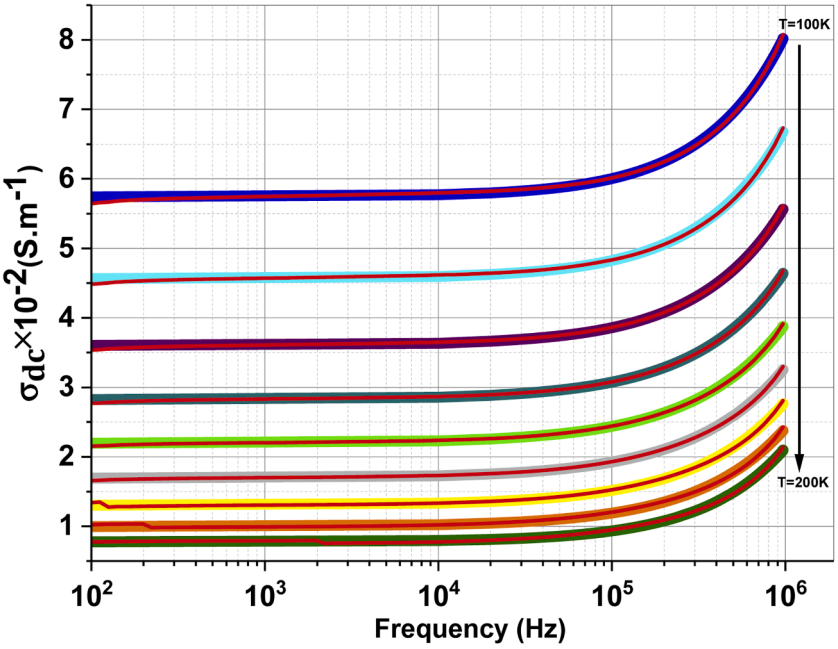

Fig. 11. Frequency dependency of the conductivity for $La_{0.57}Nd_{0.1}Sr_{0.18}Ag_{0.15}CoO_3$compound.

Where k_B is the Boltzmann constant and WM is the maximum value of the height of the potential barrier, also called ionization energy.

For sufficiently high values of $\frac{W_M}{k_B T}$ we obtain [42].

$$s = 1 - \frac{6k_B T}{W_M} \tag{7}$$

This model is the most appropriate for characterizing the electrical conduction mechanism at low temperatures. This model describes the charge carrier jumps between near-neighbor sites over a potential barrier WM that separates them.

According to the small polaron tunneling (NSPT) model, the exponent 's' increases with increasing temperature and varies with frequency according to the expression:

$$s = 1 + \frac{4}{\ln(\omega\tau) + \frac{E_a}{K_B T}} \tag{8}$$

The variation of the exponent *s* as a function of the temperatures for the sample is shown in Fig. 12. It is noted that *s* increases with the increases of the temperature. Thus, the overlapping small polaron tunneling NSPT model appears to be the most suitable one to explain the conduction mechanism in the sol-gel compound studied.

The conductivity spectra are fitted using equation (V.3). The fitting results are summarized in Table 2.

In the low frequency region, the curves indicate that our samples exhibit a semiconductor behavior in all temperature range. The *dc* electrical conductivity as a function of the temperature was analyzed using Mott's law [43]:

$$\sigma_{dc} T = B\, exp\left(-\frac{E_a}{k_B T}\right) \tag{9}$$

Where B is a pre-exponential factor, E_a is the activation energy, T is the absolute temperature and k_B is the Boltzmann constant.

The plot of $ln(\sigma_{dc})$ *vs.*$(1000/T)$ in Fig. 13 reveals a linear behavior in all the temperature ranges, confirming that the conduction process is thermally activated. The E_a values, estimated from the slope of the linear fit plots, are found to be equal to 0, 10 eV.

Table 2
Values of dcand the exponent "S".

T(K)	σ_{dc}(X10^{-5})	A(X10^{-7})	s
100	**0.45**	**2.34**	**0235**
110	**0.634**	**1.78**	**0,31**
120	**0.024**	**1.96**	**0368**
130	**0.05**	**1.24**	**0579**
140	**0.12**	**1.75**	**0634**
150	**0.4**	**9.46**	**0728**
160	**0.72**	**4.38**	**0826**
170	**0.11**	**2.698**	**0,91**
180	**2.04**	**2.99**	**0942**
190	**0.14**	**2.698**	**0972**
200	**2.08**	**2.99**	**0982**

3.5. Absorbance measurement

3.5.1. Optical band gap Eg

The fundamental processes of light absorption in materials are essential for determining their electrical properties. The UV–VIS-NIR absorbance spectra at room temperature forthe $La_{0.57}Nd_{0.1}Sr_{0.18}Ag_{0.15}CoO_3$(LNSACO) compound are shown in Fig. 14.

It is evident that the prepared sample exhibits significant absorbance in the visible range, suggesting its potential application as a photocatalytic material and for generating photovoltaic solar cells [44]. Additionally, a secondary absorption band is observed in the near-infrared region for the prepared compound, as depicted in Fig. 14. This indicates the practical utility of the compound as a promising candidate for optoelectronic devices operating in the near-infrared spectrum [45].

3.5.2. Estimation of the optical band gap energy

The optical absorption coefficient (α) can be estimated using absorbance data, in accordance with the Beer–Lambert theory using the following equation [46]:

$$\alpha = \frac{2.303 \times A}{d} \tag{10}$$

The evolution of the absorption coefficient α of our material and its derivative behavior (dα/dλ) is depicted in Fig. 15. On one hand, the

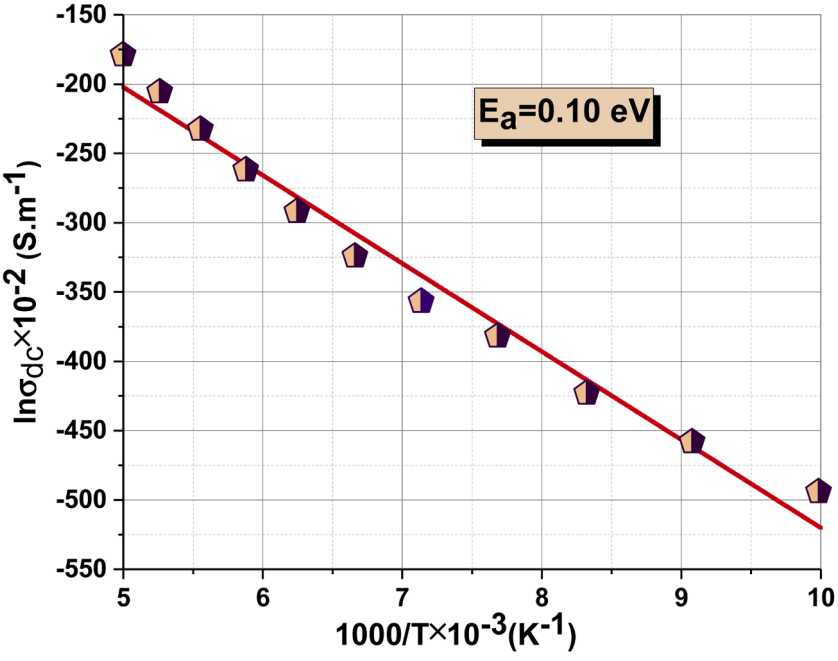

Fig. 12. The Arrhenius plots $(ln(\sigma_{dc}T)$ *vs.*$(1000/T))$ for $La_{0.57}Nd_{0.1}Sr_{0.18}Ag_{0.15}CoO_3$compound.

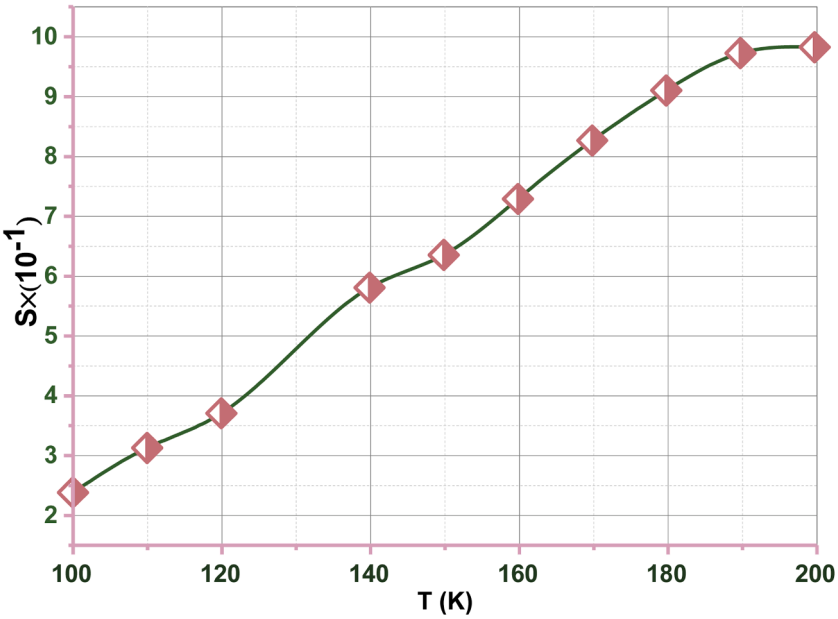

Fig. 13. Temperature dependence of the exponent *s for* $La_{0.57}Nd_{0.1}Sr_{0.18}Ag_{0.15}CoO_3$compound.

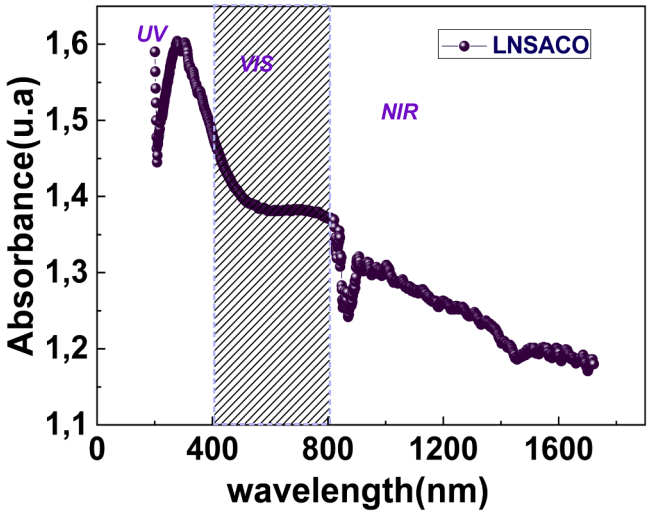

Fig. 14. the variation of absorbance spectrum as a function wavelength of LNSACO compound.

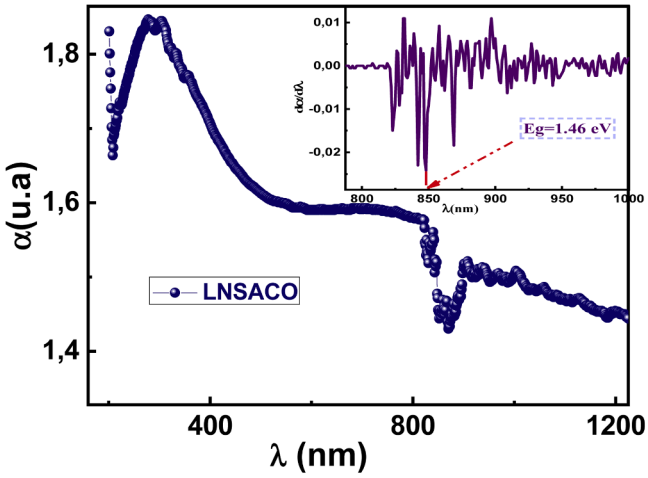

Fig. 15. the variation of the absorption coefficient (α) spectrum as a function wavelength inset the derivative of the absorption coefficient as a function wavelength of LNSACO compound.

experimental approach enables us to estimate the minimum value of dα/dλ, which is used to determine the wavelength corresponding to the bandgap (Eg)[47]. On the other hand, based on the following relation, we can calculate the band gap (Eg)value of our prepared sample [48]:

$$\left(E_g = h\nu = \frac{hc}{\lambda}\right) \tag{11}$$

where $c = 3 \times 10^8$ m/s, $h = 4.135 \times 10^{-15}$eVs. According to the dα/dλ plot, the determined λ value as λ = 848 nm. Using Eq. (7), we obtained a value of the band gap as Eg = 1.46 eV. The value of the gap energy which was found by the derivative method is confirmed by the adjusting the variation of $[(\alpha h\nu)^2$ vs. hν], Fig. 16 this adjustment gives a value Eg =1.48eV

4. Conclusion

In this work, we used the sol-gel method to synthesize the $La_{0.57}Nd_{0.1}Sr_{0.18}Ag_{0.15}CoO_3$ (LNSACO) compound, and we used XRD, EDX, SEM, and Raman spectroscopy to investigate its structural and morphological features. This chemical crystallizes in the rhombohedral system with space group R-3c, according to the XRD investigation. Nevertheless, additional peaks linked to the secondary phase of Co_3O_4 of space group Fd-3 m are visible in the XRD spectrum. Grain morphology is quite homogeneous in SEM pictures.

It was discovered that frequency and temperature had a significant impact on the electrical characteristics. The curves of electrical conductivity that adhere to Jonscher's universal power law. The NSPT model was linked to the study of ac electrical conduction. The impedance plot is characterized by semicircular arcs, and this behavior has been modeled using an equivalent electrical circuit. The identical activation energy values found from both dc conductivity (0.10 eV) and impedance spectroscopy (0.105 eV) demonstrate that the relaxation process and electrical conductivity are attributable to the same type of charge carriers. The gap energy was shown by the optical property investigation, indicating improved optoelectronic qualities of the

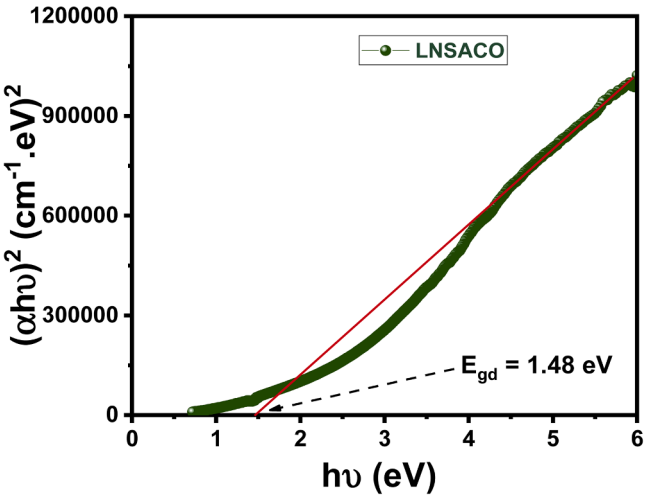

Fig. 16. the variation of the $(\alpha h\nu)^2$ as a function. $H\nu$.

produced samples.

Futures prospects

Although our study highlighted the promising characteristics of cobaltites, future research should focus on exploring a broader range of compositions to better understand structure-property relationships. Furthermore, the study of electrical conductivity and the study of doping strategies and surface modifications will contribute to improving the optoelectronic properties of these cobaltites, thus allowing their integration into various technological applications.

CRediT authorship contribution statement

T. Benslimen: Writing – original draft. **H. Issaoui:** Writing – review & editing. **M. Brahmi:** Writing – review & editing. **F. Issaoui:** Writing – review & editing, Writing – original draft. **E. Dhahri:** Methodology. **Benilde F.O. Costa:** Methodology, Formal analysis. **Bernardo A. Nogueira:** Software. **Rui Fausto:** Software, Data curation.

Declaration of competing interest

The authors have no competing interests that are relevant to the content of this article to declare.

Acknowledgements

R. F. thanks the European Research Agency (European Union) the funding through the Horizon-Widera-2023-Talents-01 ERA-Chair 1011848998: Spectroscopy@IKU “Manipulating and Characterizing Molecular Architectures: From Isolated Molecules to Molecular Crystals”.

Data availability

Upon a reasonable request, the data that support this study’s findings are available from the corresponding author.

References

[1] H. Issaoui, S. Gharbi, F. Issaoui, S. Hcini, B. Alzahrami, M.L. Bouazizi, H. Alrobei, E. Dhahri, J. Mol. Struct. 1253 (2022) 132282.
[2] O. Mentre’, et al., Solid. State Sci. 10 (2008) 471.
[3] R.H. Potze, G.A. Sawatzky, M. Abbate, Phys. Rev. B 51 (1995) 11501.
[4] M.A. Korotin, S.Y. Ezhov, I.V. Solovyev, V.I. Anisimov, D.I. Khomskii, G. A. Sawatsky, Phys. Rev. B 54 (1996) 5309.
[5] K. Knížek, P. Novák, Z. Jirák, Phys. Rev. B 71 (2005) 054420.
[6] H.-J. Lin, Y.Y. Chin, Z. Hu, G.J. Shu, F.C. Chou, H. Ohta, K. Yoshimura, S. Hébert, A. Maignan, A. Tanaka, L.H. Tjeng, C.T. Chen, Phys.Rev. B81 (2010).
[7] R.H. Potze, G.A. Sawatzky, M. Abbate, Phys. Rev. B51 (11) (1995) 501.
[8] Z. Hu, H. Wu, M.W. Haverkort, H.H. Hsieh, H.-J. Lin, T. Lorenz, J. Baier, A. Reichl, I. Bonn, C. Felser, A. Tanaka, C.T. Chen, L.H. Tjeng, Phys. Rev. Lett. 92 (2004) 207402.
[9] P. Sfirloaga, M. Stoia, M. Poienarand, P. Vlazan, Structural and opticalproperties of perovskite–type compounds obtained by ultrasonicmethod, Mat. Sci. Eng. 416 (2018) 012067, https://doi.org/10.1088/1757-899X/416/1/012067.
[10] R. Mguedla, et al., Structural, electrical, dielectric and optical properties of PPrCrO3 orthochromite, J. Alloy. Compd. 812 (2020) 152130.
[11] W. Boujelben, A.B.J. Kharrat, S. Kammoun, N. Chniba-Boudjada, K. Khirouni, W. Boujelben, Investigation of structural and optical properties of SmCrO3 orthochromite compound prepared via sol-gel process, Ion. (Kiel) (2025), https://doi.org/10.1007/s11581-025-06078-7.
[12] J. Wang, B. Wang, Z. Wang, L. Chen, C. Gao, B. Xu, Z. Jia, G. Wu, J. Colloid Interface Sci. 586 (2021) 479–490.
[13] H.M. Rietveld, J. Appl.Cryst 2 (1969) 65.
[14] N.J. Shaw, PowderMetallurgyInternational 3 (1989) 21.
[15] R.A. Young, D.B. Wiles, J. Appl. Crystallogr 14 (1981) 149.
[16] L.M. Rodriguez-Martinez, J.P. Attfield, Phys. Rev. B 54 (1996) 15622.
[17] S. Jim, Mac Cormach, T.H. Tiefel, J. Appl. Phys. 76 (1995) 10.
[18] S.R. Gawali, A.C. Gandhi, S.S. Gaikwad, J. Pant, T.S. Chan, C.L. Cheng, S.Y. Wu, Role of cobalt cations in short range antiferromagnetic Co3O4 nanoparticles: a thermal treatment approach to affecting phonon and magnetic properties, Sci. Rep. 8 (2018) 249.
[19] A.S. Ahmed, J. Gupta, A.H. Anwer, M.Z. Khan, Investigation of the dielectric and electrochemical properties of Co3O4–NiO nanocomposites with varying NiO content, Phys. B: Condens. Matter 629 (2022) 413623.
[20] V. Goldschmidt, Geochemistry, OxfordUniversityPress, 1958.
[21] E. Pollert, S. Krupička, E. Kuzmičova, J. Phys. Chem. Solid. 43 (1982) 1137.
[22] H.D. Megaw, ActaCrystallographica 5 (739) (1952).
[23] D. Kumar, A.K. Singh, J. Magn. Magn. Magn. (469) (2019) 264–273.
[24] A.P. Sazonov, I.O. Troyanchuk, V.V. Sikolenko, G.M. Chobot, H. Szymczak, J. Phys.: Condens. Matter 17 (2005) 4181–4195.
[25] D. Kumar, N.K. Verma, C.B. Singh, A.K. Singh, AIP. Conf. Proc. 1942 (2018) 050024. -4.
[26] M. Popa, L.V. Hong, M. Kakihana, Phys. B 327 (2003) 233.
[27] R.J. Wiglusz, K. Kordek, M. Małecka, A. Ciupa, M. Ptak, R. Pazik, P. Pohl, D. Kaczorowski, Dalton. Trans. 44 (46) (2015) 20067–20074.
[28] E. Barsoukov, J.R. Macdonald, Impedance Spectroscopy Theory, Experiment, and Applications, 2nd ed, John Wiley and Sons, New York, 2005.
[29] A. Benali, M. Bejar, E. Dhahri, M.F.P. Graça, L.C. Costa, J. Alloy. Compd. 653 (2015) 506.
[30] S. Hcini, A. Selmi, H. Rahmouni, A. Omri, M.L. Bouazizi, Ceram. Int. 43 (2017) 2529.
[31] H. Baaziz, N.K. Maaloul, A. Tozri, H. Rahmouni, S. Mizouri, K. Khirouni, E. Dhahri, Chem. Phys. Lett. 640 (2015) 77–81.
[32] A.R. James, K. Srinivas, Mater. Res. Bull. 34 (1999) 1301.
[33] A. Shukla, R.N.P. Choudhary, A.K. Thakur, J. Phys. Chem. Solids. 70 (2009) 1401.
[34] D. Jonhson, Software Zview 3.2. Southern Pines, Scribners Associates Inc., 2009.
[35] H. Rahmouni, B. Cherif, M. Smari, E. Dhahri, N. Moutia, K. Khirouni, Phys. B 473 (2015) 1.
[36] A.K. Jonscher, Universal Relaxation Law, Chelsea Dielectric Press, London, 1996.
[37] A. Kumar, P. Kumari, A. Das, G.D. Dwivedi, P. Shahi, K.K. Shukla, A.K. Ghosh, A. K. Nigam, K.K. Chattopadhyay, S. Chatterjee, J. Solid. State Chem. 208 (2013) 120–126.
[38] R.L. Frost, P.A. Williams, J.T. Kloprogge, P. Leverett, J. Raman Spectrosc. 32 (2011) 906–911.
[39] A. Ghosh, Phys. Rev. B 42 (1990) 5665.
[40] A.R. Long, Frequency-dependent loss in amorphous. Semiconductors,, Adv. Phys. 315 (1982) 553–637.
[41] U. Akgul, Z. Ergin, M. Sekerci, Y. Atici, Vacuum 82 (2008) 340–345.
[42] G.E. Pike, Phys. Rev. B 6 (1972) 1572.
[43] K. Funke, Prog. Solid State Chem. 22 (1993) 111.
[44] J. Wang, C. Zhang, H. Liu, et al., Spin-optoelectronic devices based on hybrid organic-inorganic trihalide perovskites, Nat. Commun. 10 (1) (2019) 129, https://doi.org/10.1038/s41467-018-07952-x.
[45] O. Rejaiba, K. Khirouni, M.H. Dhaou, et al., Investigation study of optical and dielectric paraeters using absorption and diffuse reflectance spectroscopy method on La0.57Nd0.1Sr0.13Ag0.2 MnO3 perovskite for optoelectronic application, Opt. Quant. Electron. 54 (2022) 315, https://doi.org/10.1007/s11082-022-03633-8.
[46] S.M.H. Qaid, B.A. Al-Asbahi, G.M Hamid, et al., Optical and structural properties of CsPbBr3 perovskite quantum dots/PFO polymer composite thin films, J. Colloid. Interface Sci. 563 (2020) 426–434, https://doi.org/10.1016/j.jcis.2019.12.094.
[47] A. Ben Jazia Kharrat, K. Khirouni, W. Boujelben, Electrical and optical analysis of Pr0.5−xGdxSr0.5MnO3 (x=0, 0.05, and 0.1) manganite compounds prepared via solidstate process, Ionics. (Kiel) (2023), https://doi.org/10.1007/s11581-023-05320-4 published online 01 December.
[48] R. Mguedla, J. Ben, A. Kharrat, O. Taktak, et al., Opt. Mater. 101 (2020) 109742, https://doi.org/10.1016/j.optmat.2020.109742.